MATTER: International Journal of Science and Technology
ISSN 2454-5880

Zhang et al, 2018

Volume 4 Issue 2, pp. 46-62

Date of Publication: 14th July, 2018

DOI-https://dx.doi.org/10.20319/mijst.2018.42.4662

This paper can be cited as: Zhang, Y., Zou, J., & Zheng, Y. (2018). Unsteady Characteristics Of The Shock Propagation In A Convergent Shock Tube With Small Angle. MATTER: International Journal of Science and Technology, 4(2).46-62.

UNSTEADY CHARACTERISTICS OF THE SHOCK PROPAGATION IN A CONVERGENT SHOCK TUBE WITH SMALL ANGLE

Yang Zhang
Center for Engineering and Scientific Computation, and School of Aeronautics and Astronautics, Zhejiang University, Hangzhou, Zhejiang, 310027, PR China
yangzhang@zju.edu.cn

Jianfeng Zou
Center for Engineering and Scientific Computation, and School of Aeronautics and Astronautics, Zhejiang University, Hangzhou, Zhejiang, 310027, PR China
zoujianfeng@zju.edu.cn

Yao Zheng
Center for Engineering and Scientific Computation, and School of Aeronautics and Astronautics, Zhejiang University, Hangzhou, Zhejiang, 310027, PR China
yao.zheng@zju.edu.cn

Abstract

The whole evolution of the incident shock propagation in a convergent shock tube with small angle is studied in detail by using the direct numerical simulation. Specifically, the shape of the curved shock and the unsteady flow patterns which differs from the K-H instability, have been evaluated. The results show that as a disturbance of the inclined wall on the shock, the bending position of the incident shock represents periodically changed and its non-dimensional wavelength is larger when the convergent angle becomes greater, indicating a faster response to the curvature variation. At the same time, two different flow instable patterns for the shock

propagation in the area reduction channel are discovered, one of which is the asymmetric shock bifurcations when the reflected shock from the collision of the right wall interacts with the boundary layer. This instability is closely related to the unsteady vortex shedding behind the bifurcated feet, resulting in the dramatic pressure fluctuation. Another pattern occurs when the reflected shocks generated by the curved incident shock impinge on the upper and lower walls. The collision position moves at a modest speed, which causes the formation of small vortices near the reflection regions.

Keywords

Shock/boundary Interaction, Bifurcation, Instability

1. Introduction

As a plane shock wave propagates in a channel with area reduction, its shape, strength and flow properties behind the shock are affected. Chester (1957), Chisnell (1957) and Whitham (1957, 1958) were the first to study this problem, and separately derived the one-dimensional expression of the shock Mach number and cross-sectional area. Moreover, Whitham still developed Ray-Shock theory for the two-dimensional problems and obtained an explicit equation for the local shock Mach number as a function of (α, β), and accordingly the curves of α = constant denote the shock positions, and the rays are β= constant. Subsequently, B. W. Skews (1967) studied the shape variation of the diffracting shock experimentally. A large discrepancy between the test and Ray-Shock theory is the point where the shock starts to bend, and theoretical predictions appear to be the higher curvature at low Mach number as the corner angle increases. In his works, the continuous propagation process of the diffracting shock in the channel is not considered, and the experimental analyses are not involved in the changes of the bending point with time. Igra et al. (1994) conducted a numerical verification of Whitham's approximation in area changes in a duct. Compared with the solutions of the Random Choice Method (RCM), the results of Whitham's model represent a certain deviation for higher shock Mach numbers or area reductions. It is particularly noted that the RCM solution has only first order accuracy. In addition, Sasoh et al. (1992) pointed out that the reflection mode of a weak shock seems not a simple Mach reflection, and its Mach stem is not perpendicular to the wedged surface.

In recent years, the Kelvin–Helmholtz (K-H) instabilities on shear layers in the interaction of a shock wave and a cylindrical cavity are discovered experimentally by Skews and

Kleine (2007). The complex flow features associated with shock wave reflection and focusing, such as shock systems and shear layers, are revealed in detail using high-speed video photography, and the initiation and growth of shear layers from Mach reflection or transitioned regular reflection induce the K-H instabilities eventually. Subsequently, in the research findings of Ivanov et al. (2012), the experimental and numerical results in a curved channel with reducing area illustrate three important factors, which are the intensification of shear flows, the appearance of vorticities due to pressure gradient and the density gradient along the contact surface, leading to the broken shear layers and large Kelvin-Helmholtz instabilities. Additionally, Dowse and Skews (2014) studied the post-shock flow properties for the planar shock propagating through three compound parabolic profiles with different lengths by means of experimental tests, theoretical analyses and computational fluid dynamics simultaneously. The entire evolution of wave profiles, density distributions and pressure traces behind the incident shock in the duct was presented to be three types of flow patterns, and the characteristic 'cat's eye' indicated the existence of K-H instabilities. At present, most studies about the flow instabilities in the shock propagation along a channel with area changes focus on the development of shear layers resulting from the interaction and reflection of wave system. However, the effects of boundary layer on the shock propagation for this problem are rarely concerned. Previously, a low-frequency motion in the interaction between the shock wave and turbulent boundary layer has been revealed by several researchers (Touber & Sandham, 2011; Gaitonde, 2015) and the unsteady characteristics corresponding to flow separation, vortices evolution and shock wave bending show a complex flow structure. Similarly, it is necessary to be taken the wall boundary layer into consideration due to the occurrence of the shock/boundary layer interaction as the shock gradually moves through a channel with area change.

In this paper, we numerically simulate the complete process of shock motion at Ma=1.9 by directly solving the time-dependent, compressible Navier-Stokes equations in an inclined shock tube with small angle, which is from the initial propagation of incident shock to the development of reflected normal shock owing to the collision with the right wall. Except for the attention of the shape of curved shocks, the flow instability is a key consideration from the view of the shock/boundary layer interaction. The organization of this paper is as follows. A brief review of research background and previous studies is introduced in Section 1. The numerical approach and the configuration of calculation domain are presented in Section 2, which covers the governing equations, discretization schemes, boundary condition, and etc. The discussion and

detailed analysis about the simulated results are performed in Section 3. Conclusions and future works are drawn in Section 4.

2. Mathematical formulation and numerical method

2.1 Physical model

The governing equations considered in the present simulations are two-dimensional compressible Navier-Stokes equations. We write the conservative form in the Cartesian coordinate as:

$$\frac{\partial Q}{\partial t}+\frac{\partial F_1}{\partial x}+\frac{\partial F_2}{\partial y}-\left(\frac{\partial V_1}{\partial x}+\frac{\partial V_2}{\partial y}\right)=0 \quad (1)$$

$$Q=\begin{bmatrix}\rho\\ \rho u\\ \rho v\\ \rho E\end{bmatrix} \quad F_1=\begin{bmatrix}\rho u\\ \rho u^2+p\\ \rho uv\\ \rho Hu\end{bmatrix} \quad F_2=\begin{bmatrix}\rho v\\ \rho uv\\ \rho v^2+p\\ \rho Hv\end{bmatrix} \quad (2)$$

$$V_1=\begin{bmatrix}0\\ \tau_{xx}\\ \tau_{xy}\\ u\tau_{xx}+v\tau_{xy}+q_x\end{bmatrix} \quad V_1=\begin{bmatrix}0\\ \tau_{yx}\\ \tau_{yy}\\ u\tau_{yx}+v\tau_{yy}+q_y\end{bmatrix} \quad (3)$$

where Q is the tensor of the conservative variables, and F_1, F_2, V_1, V_2 are the convective and diffusion fluxes in x and y directions, respectively. The total energy and enthalpy per unit mass are denoted by E and H.

The stress tensor τ can be expressed by

$$\tau_{xx}=2\mu\frac{\partial v}{\partial x}-\frac{2}{3}\mu\left(\frac{\partial u}{\partial x}+\frac{\partial v}{\partial y}\right) \quad \tau_{yy}=2\mu\frac{\partial v}{\partial y}-\frac{2}{3}\mu\left(\frac{\partial u}{\partial x}+\frac{\partial v}{\partial y}\right) \quad \tau_{xy}=\tau_{yx}=\mu\left(\frac{\partial u}{\partial y}+\frac{\partial v}{\partial x}\right) \quad (4)$$

The dynamic viscosity μ is obtained by the Sutherland law, which is shown as below:

$$\frac{\mu}{\mu_0}=\left(\frac{T}{T_0}\right)^{1.5}\frac{T_0+124}{T+124} \quad (5)$$

where T_0 is a reference temperature and μ_0 is the viscosity at T_0.

2.2 Numerical method

The scales of shock waves and boundary layers are within the order of millimeters. Hence, in order to predict the flow details and discover the nature of physical phenomena, a

spatially evolving DNS with high-order resolution is used to solve the two-dimensional Navier-Stoke equations. The Steger-Warming flux vector splitting method (Steger and Warming, 1981) combined with a seventh-order accurate weighted essentially non-oscillatory (WENO) scheme is used to deal with the convective terms. A sixth-order accurate central difference scheme for the diffusion terms and a three-step Runge-Kutta approach for time advancing are used. The accuracy and efficiency of the present DNS code used in this paper have been widely demonstrated and validated in the simulations of the supersonic turbulence boundary layer from Li (2005, 2009). All of the present simulations are carried out in the National Supercomputing Center of Tianhe in Guangzhou, China. In this platform, each computing node equips with two CPUs of Xeon E5 series and 12 cores, and three Xeon Phi accelerator cards of 57 cores. The memory of a single node is up to 64GB, which guarantees the high efficiency of computation.

2.3 Configuration and initial conditions

The shock propagation in an inclined channel having the geometry shown in Figure 1 is studied. The total length of computational domain is 1200mm with the initiative diameter of 76mm, which resembles the straight tube in the study of shock bifurcation from Gamezo et al. (2001). The angle γ of convergent section is 2.15 degree and the reference length L_0 of 100mm is used to non-dimensionalize this issue. For the emphasis of the unsteady features, the configuration does not impose the symmetrical condition aiming at discovering a few asymmetrical structures. We use no-slip and adiabatic boundary conditions both on the upper and lower walls. The supersonic incoming air with physical variables of ρ_0, u_0, T_0 is given to the left boundary. A planar incident shock is initially placed in X/L_0=0.55 where the distance is 200mm from the starting position of area reduction. The speed of gases in front of the shock is set to zero, and the post-shock flow parameters can be determined from the Rankine–Hugoniot conditions for a given incident Mach number Ms=1.9. In current DNS, the total number of mesh elements is 6.14×10^6. The uniform grid distribution is used in the streamwise direction, and locally refined mesh is taken into account along the normal wall. The specific flow parameters and mesh sizes are listed in Table 1.

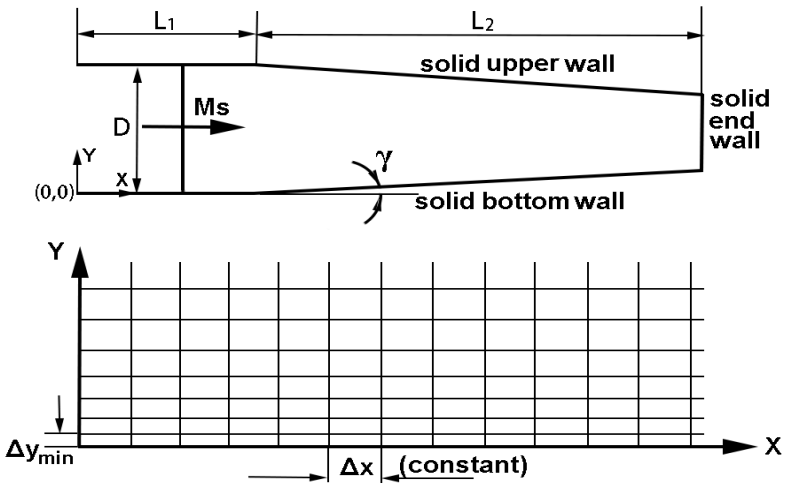

Figure 1: *Schematic of computational domain*

Table 1: *Mesh sizes & flow parameters*

Definition	Value
M_s	**1.9**
L_1	**4**
L_2	**8**
D	**0.76**
Δx	1.5×10^{-3}
$\Delta y_{\min}$	1.0×10^{-4}
L_0	**100(mm)**
ρ_0	**0.3974(kg/m^3)**
u_0	**392.977(m/s)**
T_0	**471(K)**

3. Results and discussions

3.1 Positions of the bending shock

According to Whitham's theory (1958), a direct relation between the shock Mach number and the cross-sectional area can be expressed as follows,

$$\frac{2M}{\left(M^2-1\right)K\left(M\right)}\frac{dM}{}+\frac{dA}{A}=0 \quad (6)$$

$$K\left(M\right)=2\left[\left(1+\frac{2}{\gamma+1}\frac{1-\mu^2}{\mu}\right)\left(2\mu+1+M^{-2}\right)\right]^{-1} \quad (7)$$

$$\mu^2 = \frac{(\gamma-1)M^2+2}{2\gamma M^2-(\gamma-1)} \quad (8)$$

Thus, an approximate solution M(x) can be easily obtained by solving the above equations. In figure 2, comparison between theoretical calculations using Whitham's theory and the RCM solution of Igra's work (1994), and results of the present calculation indicate good agreement, which verifies the accuracy of DNS's procedure in solving the shock propagation problem. It is worth noting that this calculation model can be regarded as a quasi-one-dimensional pattern until the shock impinges upon the right wall and causes a shock reflection due to a very small convergence angle of the channel, thus the difference of these results in the shock Mach number can be ignored.

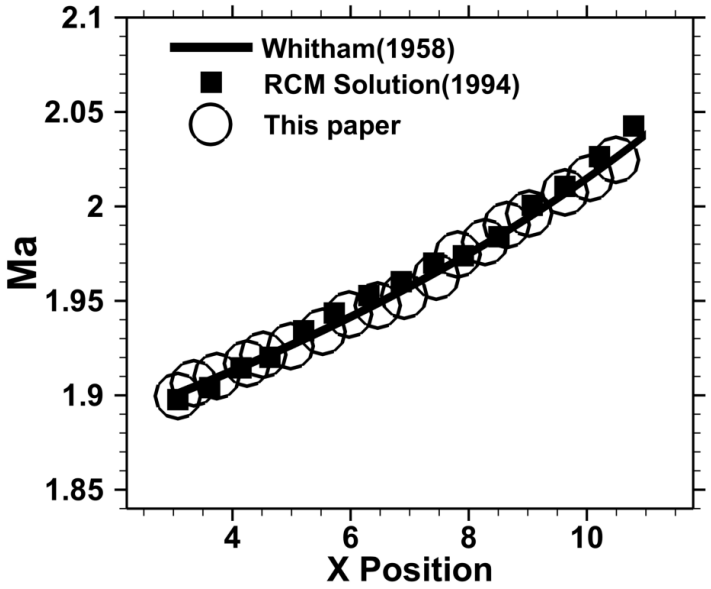

Figure 2: *Variation of the shock Mach number along an area reduction section*

The first key point which can be seen from the pressure distributions in figure 3 and 4 is that the incident shock profiles appears to be curved to some extent with plane wall shocks perpendicular to the wall and tangent to the main normal shock, even though the curvature is not obvious. But in enlarged images, from the triple points (labeled A) which represent the starting locations of the shock curvature, two reflected shocks (labeled R_S) behind the post-shock flow field are clearly identified. As the curved incident shock moves on, both two reflected shocks propagate backwards and generate a reflection by colliding with the upper and lower walls. Subsequently, two new reflected shocks exactly intersect at the symmetry plane and re-reflect off each other. Considering the effect of the supersonic inflow passing through the compression

plane, two shocks labeled T1 at the entrance do not move position significantly all the time, showing a relatively stable flow. In fact, the entire flow field structures are strictly symmetric, especially for the motions of wave system.

As mentioned earlier, in the shock diffraction experiment, Skews (1967) performed a theoretical analysis about the specific point where the shock started to bend, and a correlation of the shock Mach number and the azimuthal angle m_0 associated with the blending state was derived. However, what needs to be emphasized is that in his works, the shock behaves in a pseudo-stationary manner without consideration of the continuous propagation of the shock after the diffracting corner. For our problem, a striking result shows that the bending point of the shock remains a dynamic change due to the rapid shock propagation through the reducing channel. A schematic shape of the middle normal shock is shown in figure 5, and we have also plotted the quantitative results of the bending position until the incident shock collides with the right wall in figure 6. The most prominent feature is that the variations of two fluctuation curves present periodic even though their amplitudes are gradually decreasing. We can define a non-dimensional wave length λ using to characterize the motion of the shape of the shock, which may be considered to be a disturbance propagating from the walls to the inside owing to the area reduction of the flow passage.

$$\text{Case1: } \gamma_1 = 2.15^{\circ}, \quad \lambda_1 = 2.65$$

$$\text{Case2: } \gamma_2 = 1.07^{\circ}, \quad \lambda_1 = 2.20$$

For the comparison purpose, two cases in different convergence angles have been simultaneously simulated in order to recognize the propagating speed of disturbance determined by the area change, which is from the perspective of shock bending. It is apparent that the wave length in the larger convergence angle is relatively longer at the same shock Mach number. On the basis of the duration within one wavelength range, namely of the wave period denoted by *TT*, the speed of disturbance motion can be easily calculated as follows,

$$u = \frac{\lambda \times L_0}{TT}$$

$$\text{Case1: } u_1 = 869.76\, m/s, \quad TT\text{-}1 = 304.68\, \mu s$$

$$\text{Case2: } u_2 = 722.07\, m/s, \quad TT\text{-}2 = 304.60\, \mu s$$

Clearly, the greater the compression angle of the channel is, the faster the disturbance corresponding to the curvature variation propagates towards the internal flow region, but the periods of the fluctuations are almost identical. In practice, this deduction can also be confirmed from the farthest distance from the upper or lower wall to the bending point, which is described as the peak value of the curves in figure 6 and 7. At the case of $\gamma=2.15^0$, the two peak points at the same horizontal position in the upper and lower curves respectively are close to coincide, whereas the distance at $\gamma=1.06^0$ is approximate 0.13.

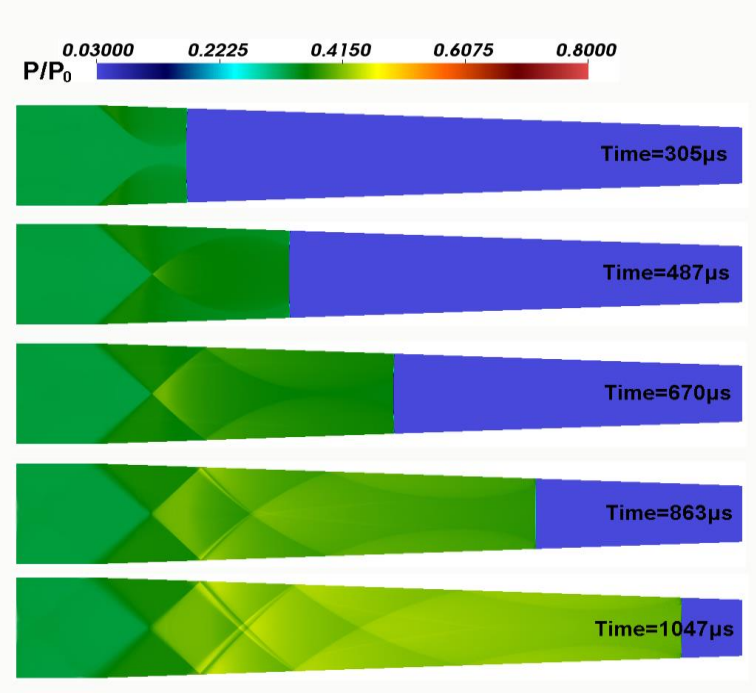

Figure 3: *Pressure contours at a series of times*

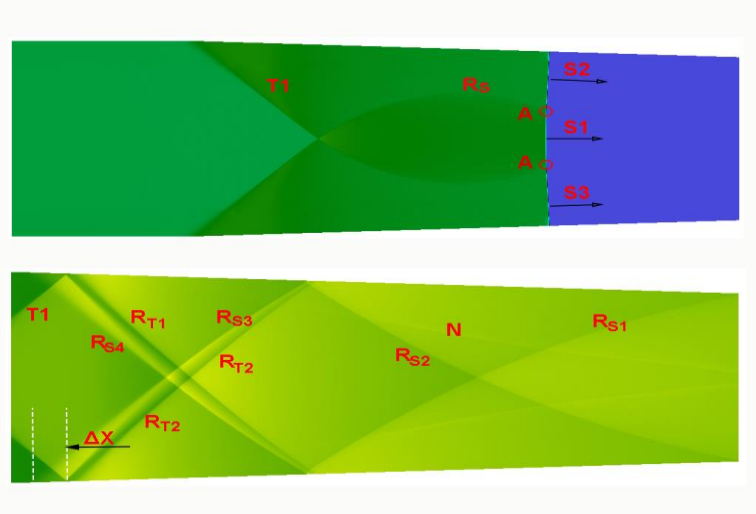

Figure 4: *Enlarged images (the upper: Time=487μs; the lower: Time=1047μs)*

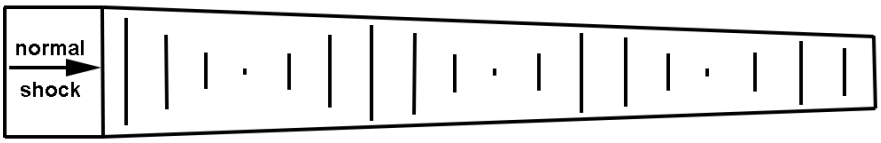

Figure 5: *Positions of the curved shock along the convergent channel*

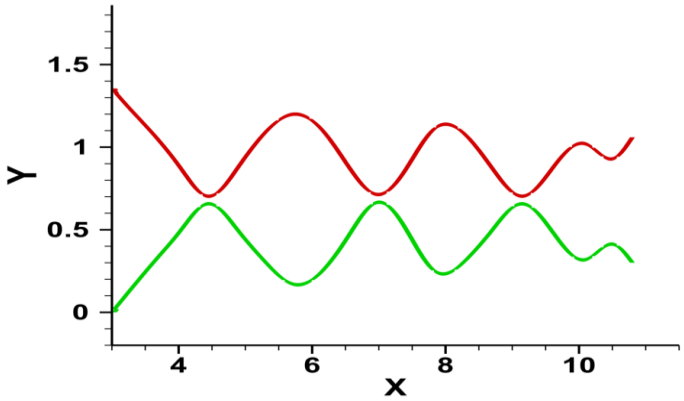

Figure 6: *Curves of bending positions at* $\gamma=2.15^0$

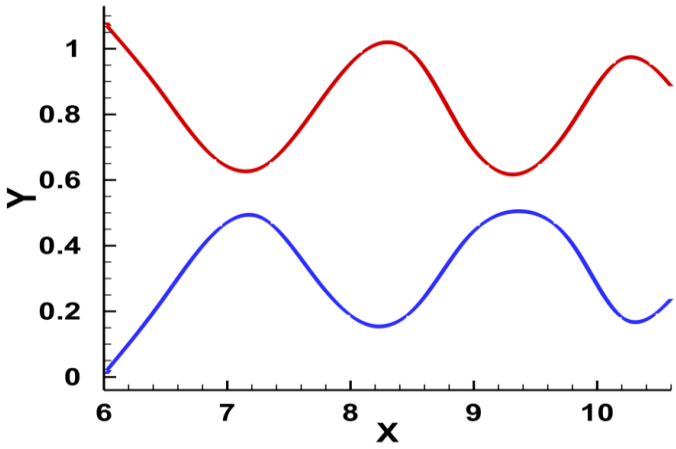

Figure 7: *Curves of bending positions at* $\gamma=1.07^0$

3.2 Unsteady flow patterns

Another focus of attention is the flow instability. From the preceding introduction it is known that K-H instabilities strongly linked with shear layers have been observed experimentally and numerically in the interactions of shock waves and curved channels. However, it is interesting to note that there exist anther unsteady flow pattern in the shock propagation mainly owing to the effects of the shock /boundary layer interaction.

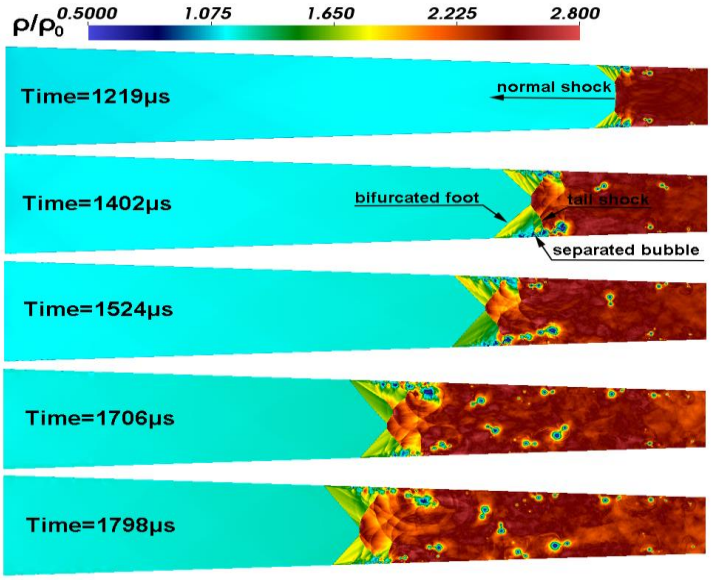

Figure 8: *Density contours of the reflected shock*

In general, as the incident shock moves to the end wall on the right, a new reflected shock will be generated and spread to the left. Based on Mark's model (1958), the shock bifurcation will occur near the wall when a reflected shock interacts with the boundary layer under certain circumstances. By means of experimental tests and numerical calculations, several investigations (Weber *et al.*, 1995; Gamezo *et al.*, 2001; Daru & Tenaud, 2009) in the past simulated the general characteristics of the bifurcation structure in shock tubes, which contained a leading bifurcated foot, a tail shock and a recirculation zone. Additionally, the bifurcated foot, the tail shock and the reflected normal shock intersect with each other at a common triple point, from which a slip line extends backward, as shown in figure 8.

Except for those basic features, an obvious flow asymmetric phenomenon that the propagation speeds of the upper and lower bifurcated feet are not synchronized can be recognized, especially at Time=1706μs. The increasingly growth of the height of the bifurcated foot brings about the area reduction of the normal shock until the two bifurcated feet meet together with a cross point, and the central position of the normal shock is not fixed. As a low speed region closely following the bifurcated foot, the impacts of separated bubbles must be the first to be considered. This is because the stable vortices are not guaranteed as the rapid spread of the reflected shock goes on. To characterize these situations thoroughly, the contours of vorticity magnitude are depicted in three moments in figure 9. The results show that a series of vortices with different sizes in the recirculation zone falls off from the upper and lower walls in succession, the mode of which is just an unsteady representation.

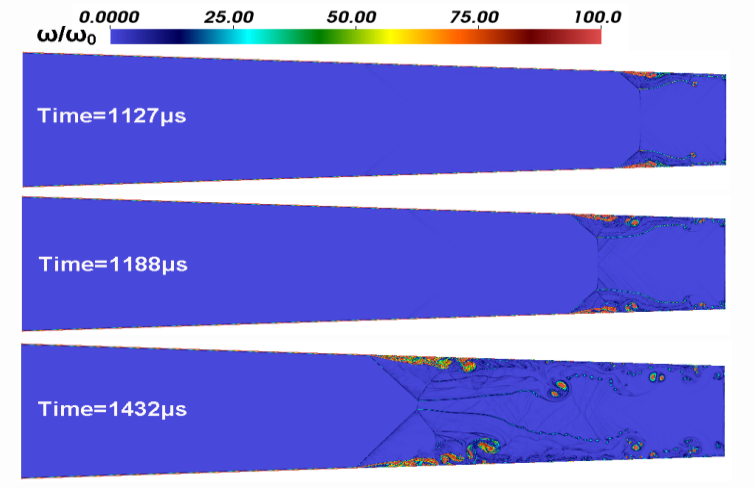

Figure 9: *The process of vortex shedding*

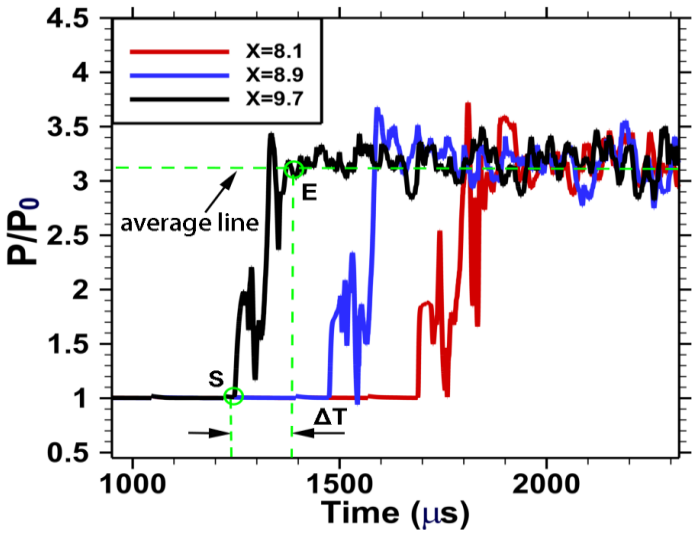

Figure 10: *Pressure fluctuations on the lower wall*

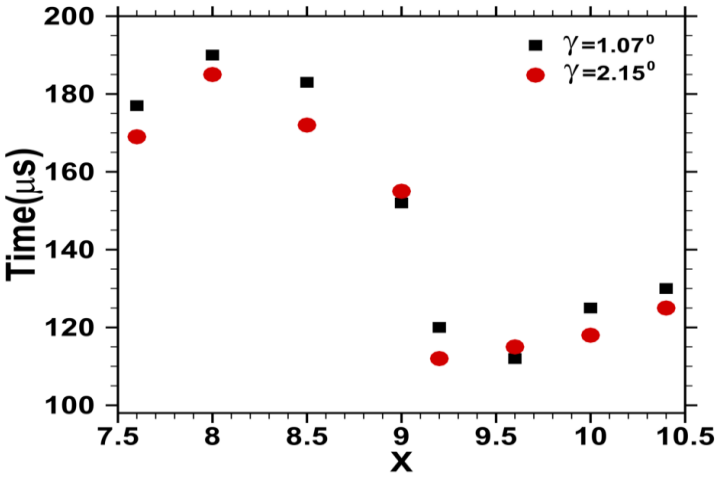

Figure 11: *The shedding period of vortex*

Starting from shock reflection, the pressure changes in three positions of the lower wall have been monitored and the fluctuating curves are shown in figure 10. The amplitude experiences an immediate jump at the moment of S as the reflected shock is approaching, and subsequently a large pressure fluctuation happens from S moment to E moment as a result of the continuous development of the vortices in the recirculation zone including the initial production, rapid growth and ultimate shedding. In order to quantitatively characterize the shedding motion, the duration of S moment to E moment can be roughly taken as the vortex shedding period. The point E can be determined by the average line which represents the time-average value of small pressure fluctuations in a relatively long time after the vortex shedding. We plot the situations of the vortex shedding period in both case 1 and 2 in figure 11. It can be found that these periods fluctuate up and down from 110μs to 190μs with the reflected shock propagating forwards, combined with the large pressure leap in the recirculation zone, which commonly leads to the asymmetric structures of shock bifurcations. Clearly, this flow instability is closely related to the effects of the boundary layer, which differs from the K-H instability.

Previously mentioned in the discussions of the incident shock propagation, at the points where the incident shock is bent, two new reflected shocks labeled R_S gradually extend backwards and encounter multiple reflections and collisions with the walls and the central plane. The most important is that these reflected shocks system are not fixed but always in motion to spread backwards when the curved incident shock rapidly propagates along with the contraction channel, as shown in figure 4. To describe this motion, we choose the stable shock labeled R_{T2} from the reflection of the inlet shock T2 as a position reference, and obtain the correlation between the displacements of reflected shocks R_S with time, which is almost linear and can be gained an approximate speed of U_R=16.39m/s by the expression of $U_R = \Delta x/\Delta T$.

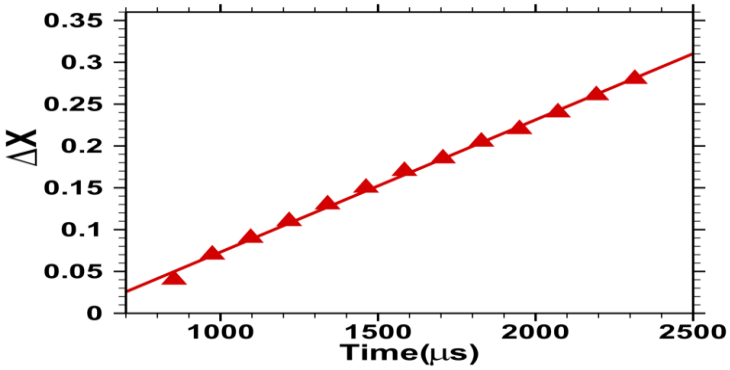

Figure 12: *The reflected shocks R_S movement with time*

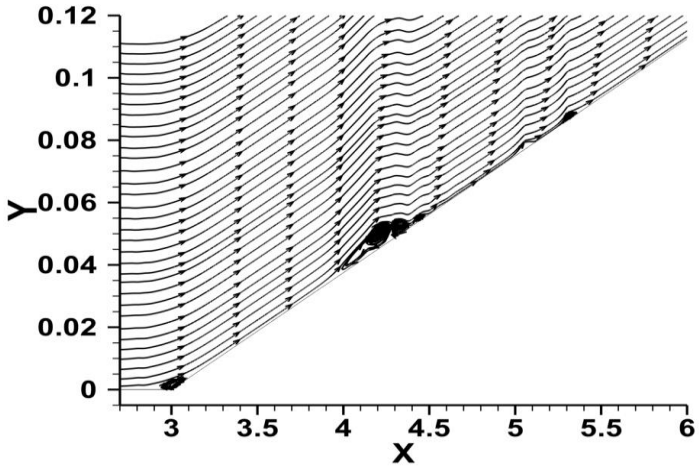

Figure 13: *Local vortices with small sizes*

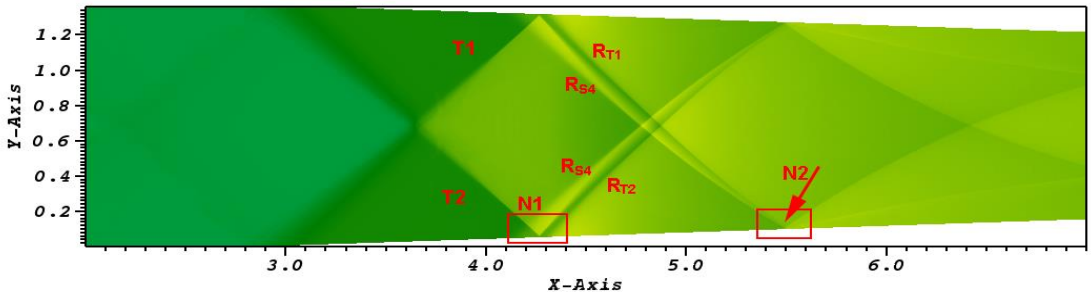

Figure 14: *Positions of small vortices*

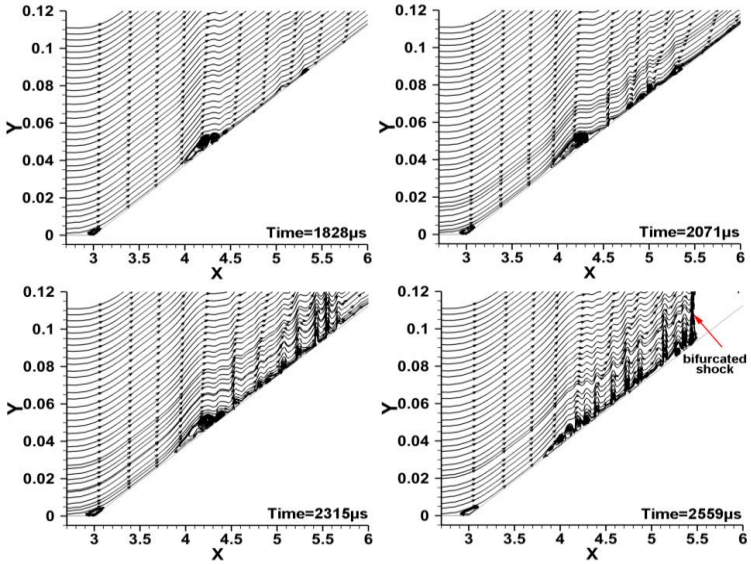

Figure 15: *Evolution of vortices with time*

As the reflected shocks R_S propagate towards the left at a low speed, it is interesting to note that there exists one or two small recirculation regions attached to the wall, where their

places exactly locate in the impact points of the reflected shocks with the walls, as shown in figure 13 and 14. Initially, just one small size of vortex occurs near the zone of N1 approximately between X=4 and X=4.5. Subsequently, the smaller vortices corresponding to the initial vortex start to grow and move to the left in a modest rate. Eventually at Time=2559μs, the vortices take up most of the area from X=4 to X=5.6 and the streamlines become extremely distorted due to the shock bifurcation. By the analyses of local vortices on the front walls, it can be conclude that the motion of reflected shocks R_S near the collision points represents quite unsteady and their interactions with the boundary layers induce several vortices with small sizes generated near the walls, resulting in the further instability for the whole flow field.

4. Conclusions

In this paper, a direct numerical simulation of the shock propagation in a convergent shock tube with small angle is carried out at Ma=1.9. The interaction of the reflected shock and boundary layer closely associated with the unsteady flow motion has been preliminarily explored. A few findings can be obtained:

1) Due to the area reduction, the incident shock in the propagation will bend and its bending position represents periodically changed. The non-dimensional wavelength of the fluctuation curve is larger as the convergent angle becomes greater, which indicates that this disturbance propagating towards the internal flow is accelerating.
2) The first flow instability represents the asymmetric shock bifurcation as the reflected shock generated by the collision with the right wall happens to interact with the boundary layer. Its mechanism is strongly associated with the vortex shedding.
3) Another instability pattern occurs when the reflected shocks behind the incident shock impinge on the upper and lower walls. The movement of the collision points directly induces the formation of many small vortices near the reflection region.

References

Chester, W. (1953). The propagation of shock waves in a channel of non-uniform width. The Quarterly Journal of Mechanics and Applied Mathematics, 6(4), 440-452. https://doi.org/10.1093/qjmam/6.4.440

Chisnell, R. F. (1957). The motion of a shock wave in a channel, with applications to cylindrical and spherical shock waves. Journal of Fluid Mechanics, 2(3), 286-298. https://doi.org/10.1017/S0022112057000130

Daru, V., & Tenaud, C. (2009). Numerical simulation of the viscous shock tube problem by using a high resolution monotonicity-preserving scheme. Computers & Fluids, 38(3), 664-676. https://doi.org/10.1016/j.compfluid.2008.06.008

Davies, L., & Wilson, J. L. (1969). Influence of Reflected Shock and Boundary‐Layer Interaction on Shock‐Tube Flows. The Physics of Fluids, 12(5), I-37. https://doi.org/10.1063/1.1692625

Dowse, J., & Skews, B. (2014). Area change effects on shock wave propagation. Shock Waves, 24(4), 365-373. https://doi.org/10.1007/s00193-014-0501-z

Gaitonde, D. V. (2015). Progress in shock wave/boundary layer interactions. Progress in Aerospace Sciences, 72, 80-99. https://doi.org/10.1016/j.paerosci.2014.09.002

Gamezo, V. N., Khokhlov, A. M., & Oran, E. S. (2001). The influence of shock bifurcations on shock-flame interactions and DDT. Combustion and flame, 126(4), 1810-1826. https://doi.org/10.1016/S0010-2180(01)00291-7

Helmholtz instability on shock propagation in curved channel. In 15th International Symposium on Flow Visualization, ISFV-15, Minsk, Paper (Vol. 177).

Hui, G., De-Xun, F., Yan-Wen, M., & Xin-Liang, L. (2005). Direct numerical simulation of supersonic turbulent boundary layer flow. Chinese Physics Letters, 22(7), 1709. https://doi.org/10.1088/0256-307X/22/7/041

Igra, O., Elperin, T., Falcovitz, J., & Zmiri, B. (1994). Shock wave interaction with area changes in ducts. Shock waves, 3(3), 233-238. https://doi.org/10.1007/BF01414717

Ivanov, I. E., Dowse, J. N., Kryukov, I. A., Skews, B. W., & Znamenskaya, I. A. (2012). Kelvin-

Mark, H. (1958). The interaction of a reflected shock wave with the boundary layer in a shock tube. National Advisory Committee for Aeronautics.

Sasoh, A., Takayama, K., & Saito, T. (1992). A weak shock wave reflection over wedges. Shock Waves, 2(4), 277-281. https://doi.org/10.1007/BF01414764

Skews, B. W. (1967). The shape of a diffracting shock wave. Journal of Fluid Mechanics, 29(2), 297-304. https://doi.org/10.1017/S0022112067000825

Skews, B. W., & Kleine, H. (2007). Flow features resulting from shock wave impact on a cylindrical cavity. Journal of Fluid Mechanics, 580, 481-493. https://doi.org/10.1017/S0022112007005757

Steger, J. L., & Warming, R. F. (1981). Flux vector splitting of the inviscid gasdynamic equations with application to finite-difference methods. Journal of computational physics, 40(2), 263-293. https://doi.org/10.1016/0021-9991(81)90210-2

Touber, E., & Sandham, N. D. (2011). Low-order stochastic modelling of low-frequency motions in reflected shock-wave/boundary-layer interactions. Journal of Fluid Mechanics, 671, 417-465. https://doi.org/10.1017/S0022112010005811

Xin-Liang, L., De-Xun, F., Yan-Wen, M., & Hui, G. (2009). Acoustic calculation for supersonic turbulent boundary layer flow. Chinese Physics Letters, 26(9), 094701. https://doi.org/10.1088/0256-307X/26/9/094701

Weber, Y. S., Oran, E. S., Boris, J. P., & Anderson Jr, J. D. (1995). The numerical simulation of shock bifurcation near the end wall of a shock tube. Physics of Fluids, 7(10), 2475-2488. https://doi.org/10.1063/1.868691

Whitham, G. B. (1957). A new approach to problems of shock dynamics Part I Two-dimensional problems. Journal of Fluid Mechanics, 2(2), 145-171. https://doi.org/10.1017/S002211205700004X

Whitham, G. B. (1958). On the propagation of shock waves through regions of non-uniform area or flow. Journal of Fluid Mechanics, 4(4), 337-360. https://doi.org/10.1017/S0022112058000495